







Article

Immobilised rGO/TiO₂ Nanocomposite for Multi-Cycle Removal of Methylene Blue Dye from an Aqueous Medium

Martina Kocijan ^{1,*} , Lidija Čurković ^{1,*} , Igor Bdikin ² , Gonzalo Otero-Irurueta ² , María J. Hortigüela ² , Gil Gonçalves ² , Tina Radošević ³, Damjan Vengust ⁴ and Matejka Podlogar ^{3,5,*}

- ¹ Department of Materials, Faculty of Mechanical Engineering and Naval Architecture, University of Zagreb, Ivana Lučića 5, 10000 Zagreb, Croatia
- ² Centre for Mechanical Technology and Automation (TEMA), Mechanical Engineering Department, University of Aveiro, 3810-193 Aveiro, Portugal; bdikin@ua.pt (I.B.); otero.gonzalo@ua.pt (G.O.-I.); mhortiguela@ua.pt (M.J.H.); ggconcalves@ua.pt (G.G.)
- ³ Department for Nanostructured Materials, Jožef Stefan Institute, Jamova Cesta 39, SI-1000 Ljubljana, Slovenia; tina.radošević@ijs.si
- ⁴ Advanced Materials Department, Jožef Stefan Institute, Jamova Cesta 39, SI-1000 Ljubljana, Slovenia; damjan.vengust@ijs.si
- ⁵ Department of Chemical Engineering and Technical Safety, Faculty of Chemistry and Chemical Technology, University of Ljubljana, Večna Pot 113, SI-1000 Ljubljana, Slovenia
- * Correspondence: martina.kocijan@fsb.hr (M.K.); lidija.curkovic@fsb.hr (L.Č.); matejka.podlogar@ijs.si (M.P.)

Abstract: This work presents the immobilisation of titanium dioxide (TiO₂) nanoparticles (NPs) and reduced graphene oxide (rGO)-TiO₂ nanocomposite on glass sheets for photocatalytic degradation of methylene blue (MB) under different radiation sources such as ultraviolet and simulated solar radiation. The TiO₂ NPs and rGO-TiO₂ nanocomposite were synthesised through a simple hydrothermal method of titanium isopropoxide precursor followed by calcination treatment. Deposition of prepared photocatalysts was performed by spin-coating method. Additionally, ethylene glycol was mixed with the prepared TiO₂ NPs and rGO-TiO₂ nanocomposite to enhance film adhesion on the glass surface. The photocatalytic activity under ultraviolet and simulated solar irradiation was examined. Further, the influence of different water matrices (milli-Q, river, lake, and seawater) and reactive species (h⁺, •OH, and e⁻) on the photocatalytic efficiency of the immobilised rGO/TiO₂ nanocomposite was carefully assessed. MB dye photocatalytic degradation was found to increase with increasing irradiation time for both irradiation sources. The immobilisation of prepared photocatalysts is very convenient for environment applications, due to easy separation and reusability, and the investigated rGO/TiO₂-coated glass sheets demonstrated high efficiency in removing MB dye from an aqueous medium during five consecutive cycles.

Keywords: reduced graphene oxide; nanocomposite; photocatalysis; methylene blue; water matrix



Citation: Kocijan, M.; Čurković, L.; Bdikin, I.; Otero-Irurueta, G.; Hortigüela, M.J.; Gonçalves, G.; Radošević, T.; Vengust, D.; Podlogar, M. Immobilised rGO/TiO₂ Nanocomposite for Multi-Cycle Removal of Methylene Blue Dye from an Aqueous Medium. *Appl. Sci.* **2022**, *12*, 385. <https://doi.org/10.3390/app12010385>

Academic Editors: David G. Calatayud and Boyang Mao

Received: 28 October 2021

Accepted: 27 December 2021

Published: 31 December 2021

Publisher's Note: MDPI stays neutral with regard to jurisdictional claims in published maps and institutional affiliations.



Copyright: © 2021 by the authors. Licensee MDPI, Basel, Switzerland. This article is an open access article distributed under the terms and conditions of the Creative Commons Attribution (CC BY) license (<https://creativecommons.org/licenses/by/4.0/>).

1. Introduction

Microorganic pollutants are increasingly more commonly found throughout environmental water systems. Although small in quantity, these unnatural elements could have a harmful impact on living organisms in the ecosystem and can negatively impact the ecological balance. The textile industry plays an important role in the developing world; however, it is also associated with increased pollution. According to the latest research, textile industry releases wastewater containing harmful chemicals such as dyes, acids, alkalis, surfactants, hydrogen peroxide, etc., throughout several processing steps [1,2]. It is responsible for generation of 20% wastewater in comparison to remaining industry sectors [3,4]. Hence, new processing solutions have been proposed in order to reduce wastewater generation. The proposed solutions need to be improved due to generation of toxic by-products [1]. Increasingly more attractive are purification processes that consider

catalysts in the advanced oxidation processes (AOPs). These are especially effective against organic macromolecules of contaminants commonly used as colouring agents. Most studied is probably methylene blue, which is still widely used despite being carcinogenic [5].

Catalytic materials that can be applied in the AOPs for environmental remediation are commonly graphene-based materials because of their characteristic high surface area, physicochemical and mechanical strength, thermal and electron mobility, etc. [6–8]. A simple and low-cost approach to preparing graphene-based materials is to synthesise graphene oxide (GO) from the chemical exfoliation of commercial graphite flakes. GO is an oxidised form of graphene material with several oxygen functional groups such as epoxy, carbonyl, carboxyl, and hydroxyl, which also assists the catalysis. The physicochemical properties of GO can significantly change because the oxidation process also introduces defects into the carbon structure [9,10]. Another related compound is reduced graphene oxide (rGO) which has a lower content of oxygen functional groups than GO nanosheets, while the overall properties are closer to graphene. Together with graphene-based material, researchers also consider a composite which also includes nanosized semiconductors. AOPs of such compounds depend on the interaction between both [11,12]. Two methods that are commonly considered for the purification of water, using these types of materials, are namely absorption and photocatalysis [13–16]. While absorption is fast, organic pollutants cannot be completely removed from aquatic environments if they have abounded. Thus, photocatalysis is more appropriate for the thorough degradation of organic pollutants [10,17–19]. rGO material in the TiO₂-rGO nanocomposite can reduce the electron-hole recombination in TiO₂. Thus, the charge transfer rate of electrons increases as well as adsorbed amount of materials at the surface, which contributes to the enhancement of the photocatalytic activity of the nanocomposite compared to the pure TiO₂ nanoparticles [20,21].

Many existing reactors involve suspension of prepared rGO/TiO₂ nanoparticles in an aqueous medium, providing large surface area for the reaction, which is very effective. Fine particles of photocatalyst can be used in the form of suspension or it can be immobilised on various substrates by different methods. Different immobilisation routes have been utilised to cover substrates by fine particles of photocatalyst such as glass [22], polymer [23], zeolite [24], cellulose [25], ceramic [26–28], and magnetic particles [29–31]. Immobilisation of fine particles of photocatalyst on the surface of the substrate eliminates the need for complicated separation of the photocatalyst from the treated water.

The aim of this study is to optimise the suspension parameters of the spin-coating method for rGO/TiO₂ nanocomposite immobilisation on the glass substrate. Methylene blue (MB) dye aqueous solution was used as a model organic pollutant in milli-Q water and three real environmental water samples (river water, lake water, and sea water). The adsorption, as well as photocatalytic activity of prepared nanocomposite material, was investigated in real environmental water samples. The criteria to meet the necessary requirements for practical application were strong adhesion on the glass substrate and effective degradation performance. To investigate the effectiveness of immobilised photocatalyst in the removal of MB dye, five successive cycles were employed. The immobilised rGO/TiO₂ nanocomposite exhibits an improved effective removal of MB as well as better adhesion when compared with pure TiO₂ catalyst, which was also fixed on a glass substrate as a reference. In addition, with this study we also revealed which functional groups assists the degradation of MB more.

2. Materials and Methods

2.1. Materials

Acetylacetone (CH₃(CO)CH₂(CO)CH₃) and methylene blue were supplied by VWR Chemicals GmbH (Dresden, Germany). Hydrochloric acid (HCl, 37%), potassium permanganate (KMnO₄), sodium nitrate (NaNO₃), hydrogen peroxide (H₂O₂, 30% *w/v*), graphite flakes (≤50 μm), titanium (IV) isopropoxide (Ti(C₃H₅O₁₂)₄, TTIP, 97%), *i*-propanol (C₃H₇OH), ethylenediaminetetraacetic acid disodium salt dihydrate (EDTA-2Na), ethylene glycol (C₂H₆O₂), and silver nitrate (AgNO₃) were purchased from Merck KGaA (Darm-

stadt, Germany). The ultrapure water was produced in a LaboStar[®] PRO water purification system (resistivity 18.2 MΩ/cm at 24.5 °C, 0.2 µm sterile filter, Siemens).

2.2. Synthesis of GO, TiO₂, and rGO/TiO₂

The GO was prepared following the previously reported chemical synthesis [16]. Briefly, 3 g of graphite flakes was dispersed in 69 mL of sulfuric acid and 1.5 g of sodium nitrate. After obtaining a homogeneous mixture and a temperature below 5 °C was achieved in an ice bath, the 9 g of potassium permanganate was added gradually. Afterward, the mixture was heated at 35 °C for 30 min and milli-Q water was slowly added. Then, the temperature of the mixture was heated up to 98 °C and held for the next 15 min. At the end of the reaction, the mixture was cooled at room temperature and 420 mL of milli-Q water and 3 mL of hydrogen peroxide (30%) were added. The resultant material was centrifuged (10 min, 3000 rpm) to remove the impurities and isolate the GO nanosheets. To purify the GO nanosheets, the mixture was washed several times with hydrochloric acid (10 wt.%) and milli-Q water until neutral pH was reached.

TiO₂ colloidal solution was prepared using the following reagents: titanium (IV) isopropoxide as a precursor, *i*-propanol as a solvent, acetylacetone as a chelating agent, and nitric acid as a catalyst [32].

According to the procedure previously reported and the obtained results [16], the selected amount of the synthesised GO suspension (10 wt.%) was added to the TiO₂ sol. To acquire homogeneous dispersion, the suspension was ultrasonicated for 15 min and then transferred to the Teflon-lined autoclave for hydrothermal synthesis (6 h at 180 °C). Afterward, resulting nanocomposite in the powder form was recovered by centrifuging at 3000 rpm from the supernatant and was washed with the ethanol and milli-Q water. For comparison, the same procedure, as applied for the preparation of rGO/TiO₂, was adopted to prepare pure TiO₂ nanoparticles, but without adding GO. The synthesised pure TiO₂ and rGO/TiO₂ nanocomposite was annealed at 300 °C with a heating rate of 3 °C/min and 2 h dwelling time, then cooled naturally to room temperature.

2.3. Preparation of Immobilised TiO₂ and rGO/TiO₂ Nanocomposite

The transparent glass sheets (20 mm × 25 mm × 1 mm) were treated in isopropanol and milli-Q water for 15 min in an ultrasonic bath to eliminate impurities from the glass surface. Then, the glass sheets were dried in an oven at 50 °C for 1 h. The prepared catalyst and ethylene glycol were mixed in the appropriate ratio. The mixture was stirred and transferred into an ultrasonic bath at room temperature for 15 min to obtain a homogeneous suspension, which was drop-casted on the surface of a glass and immobilised by spin-coating (WS-400-6NPP Laurell Technologies, USA) technique at 1500 rpm for 20 s. The glass substrates covered with catalysts were dried in an oven at 105 °C for 15 min. The homogeneous surface coverage of glass substrate was achieved after three layers of catalyst.

2.4. Characterisation

Morphology and surface analysis was conducted with a scanning electron microscope JEOL JSM-7600F. UV-Vis diffuse reflectance spectra (DRS) were obtained in the measurement range of 200–700 nm at room temperature. The samples were analysed with a UV-3600 spectrophotometer (Shimadzu, Kyoto, Japan) equipped with a reflectance sphere.

2.5. Photocatalytic Experiment

The MB solution was prepared using milli-Q water. The initial concentration was 5 mg/L. In total, 30 mL of the prepared MB solution was added to a quartz reactor with immobilised glass substrates. The adsorption-desorption equilibrium was conducted in the dark for 1 h. Then, the irradiation was turned on and aliquots (220 µL) were collected in intervals of 30 min and the absorbance was monitored by UV-Vis spectroscopy on a Lambda 950 UV/VIS/NIR spectrophotometer (PerkinElmer, Waltham, MA, USA) in the 400–700 nm range using quartz cuvette (Hellma Analytics, Stuttgart, Germany) with a path

length of 10 mm. The photocatalytic activity was investigated under ultraviolet A (UV-A) lamp (Supratec 18W/73, Osram) with a specified wavelength between 300 and 400 nm and a simulated solar lamp (Osram Ultra Vitalux 300W). The solution was stirred continuously with magnetic stirrer at 350 rpm for better homogenisation at a 15 cm distance from the light source.

To determine the influence of possible catalytic species on the degradation process, different scavengers were utilised: 10 mol L⁻¹ of EDTA-2Na, silver nitrate (AgNO₃), and isopropanol (IPA) was added to the MB solution to catch hydroxyl radical hole (h⁺), electron (e⁻), and (•OH), respectively [33,34].

To better simulate realistic conditions for possible water remediation, we also investigated the process in different water environments which were collected from river, lake, and sea. River water was collected at the source of the Soča river. Lake water was taken from Bled and seawater was collected on the coast near the city of Piran.

The ability to reuse the glass functionalised with nanocomposite for removal of MB from the aqueous medium was evaluated after five consecutive cycles. After each performed photocatalytic test, the immobilised rGO/TiO₂ nanocomposite was washed with absolute ethanol and milli-Q water and then dried at room temperature over the night.

3. Results and Discussion

To evaluate the adhesion of the immobilised photocatalyst on glass sheets, immobilised photocatalyst was exposed to milli-Q water under stirring over the night. No visual leaching of photocatalysts into the water was observed. The immobilised glass sheets with rGO/TiO₂ nanocomposite (A) and pure TiO₂ (B) are shown in Figure 1.

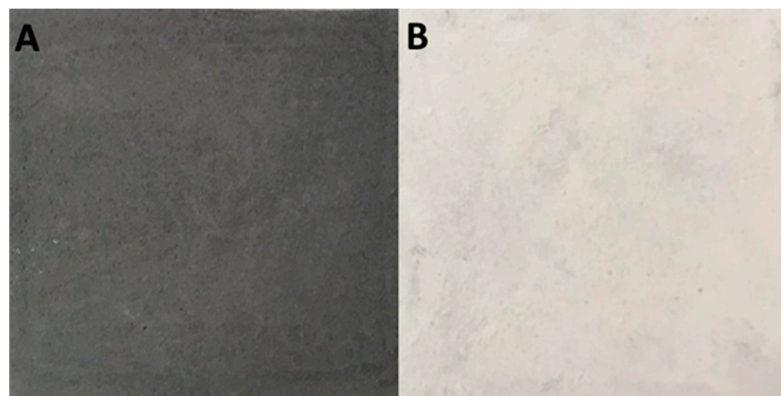


Figure 1. Picture of immobilised (A) rGO/TiO₂ nanocomposite and (B) pure TiO₂.

3.1. Composition and Morphology

Figure 2 presents the SEM images of the surface of the photocatalysts coated on glass sheets before the photocatalytic tests. The rough surface morphology of immobilised photocatalysts and appearance of assembled agglomerates of as-prepared photocatalysts of pure TiO₂ and rGO/TiO₂ nanocomposite are observed as shown in Figure 2A,B, respectively.

The optoelectronic properties were measured by DRS in the UV-Vis, as shown in Figure 3. The band gap energy (E_g) is calculated using Kubelka–Munk transformation: $(F(R) \times hv)^{\frac{1}{n}} = C(hv - E_g)$, where n is the constant for the type of optical transition and its value is 2 for permitted indirect transition [35]. The E_g values are determined from plotted graphs. E_g of the pure TiO₂ was determined to be 3.18 eV (Figure 3A), whereas the band gap for the rGO/TiO₂ nanocomposite was 2.87 eV (Figure 3B). The observed reduction in the band gap energy is a result of the inclusion of rGO material into the nanocomposite. These results indicate that the optical characteristics of TiO₂ are strongly influenced by the presence of rGO nanosheets and an increased amount of rGO narrows the band gap in nanocomposite materials. According to the literature, this result can

be assigned to the formation of Ti–O–C covalent bonds in the nanocomposites during hydrothermal synthesis [35,36].

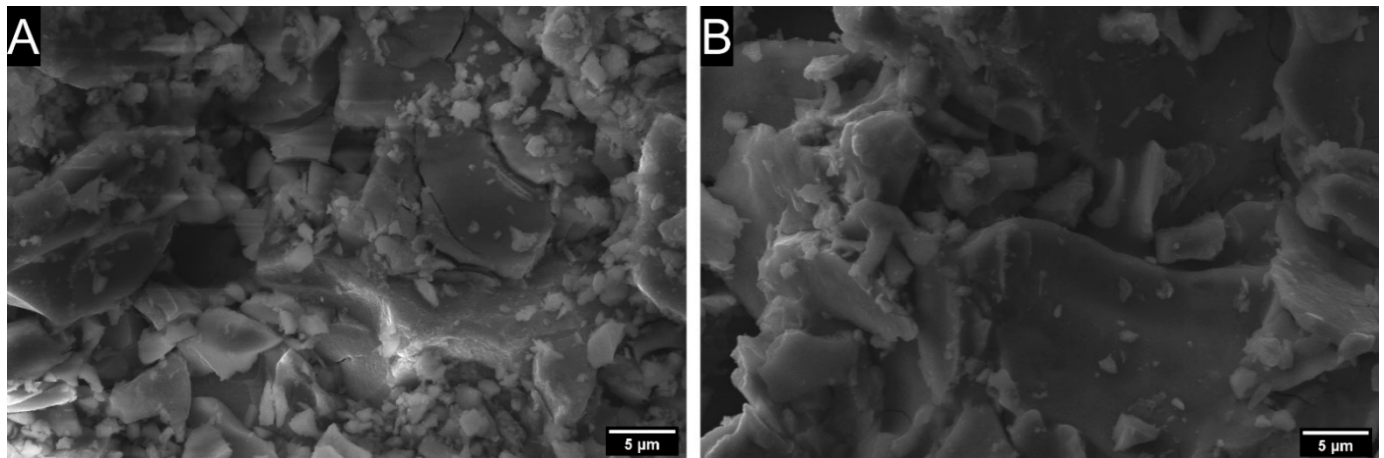


Figure 2. SEM images of immobilised (A) TiO₂ and (B) rGO/TiO₂ on surface of glass substrate before use.

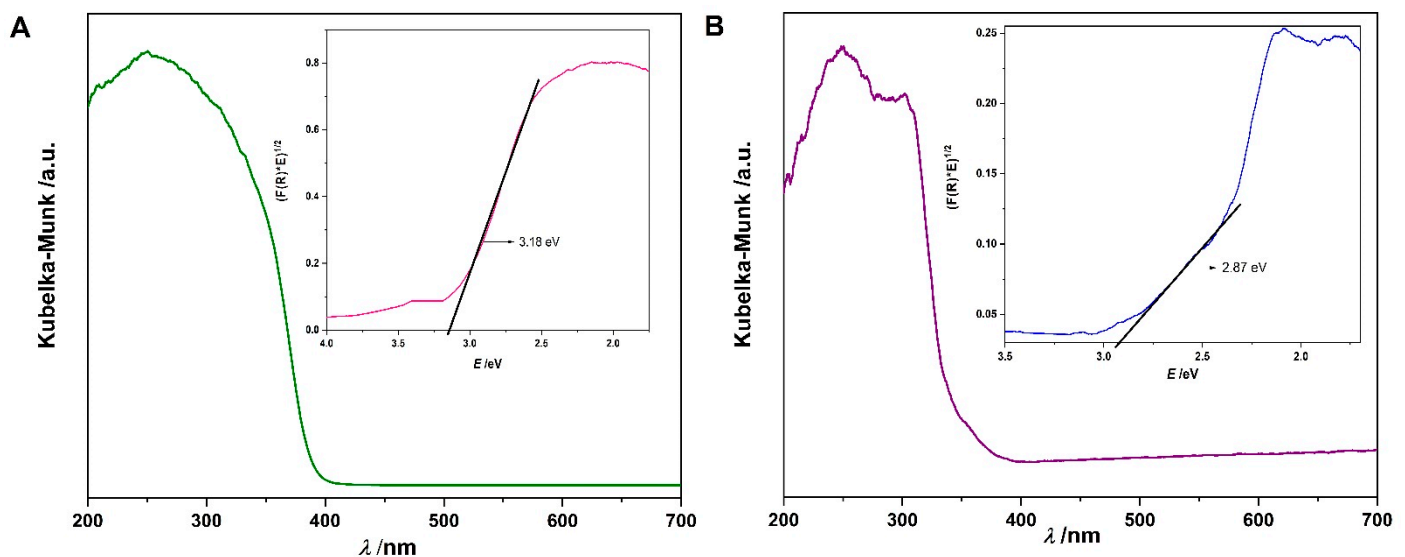


Figure 3. Diffuse reflectance UV-Vis spectra of (A) pure TiO₂ and (B) rGO/TiO₂ nanocomposite. Insets are corresponding plots of transformed Kubelka–Munk function versus the energy of the light for as-prepared photocatalysts.

3.2. Photocatalytic Performance

The results of the photocatalytic activity of the two different samples are presented next. Comparison of obtained results of adsorption, photolysis, and photocatalysis degradation of MB dye from an aqueous medium (milli-Q water) under simulated solar light irradiation and also under UV-A irradiation are presented in Figure 4A. Photolytic and photocatalytic performance for the degradation of MB over immobilised rGO/TiO₂ nanocomposite, bare TiO₂, and without catalyst under ultraviolet and simulated solar irradiation is presented. To clarify the effect of direct photolysis of MB dye, the photolytic tests were performed under both sources of irradiation. It can be seen from Figure 4B that only ~11.5% of MB dye is degraded from an aqueous medium (milli-Q water) after 120 min of simulated solar irradiation without presence of catalyst. There is no photolytic degradation of MB dye under UV-A irradiation. The UV-A irradiation did not provide enough energy to degrade a complex organic pollutant such as MB dye. On the other hand, when the MB

dye was exposed to the photolysis with the simulated solar irradiation, it exhibited a slight degradation. The simulated solar irradiation is probably more efficient by providing a higher energy density and is therefore more suitable for the degradation of complex organic pollutants such as MB [37].

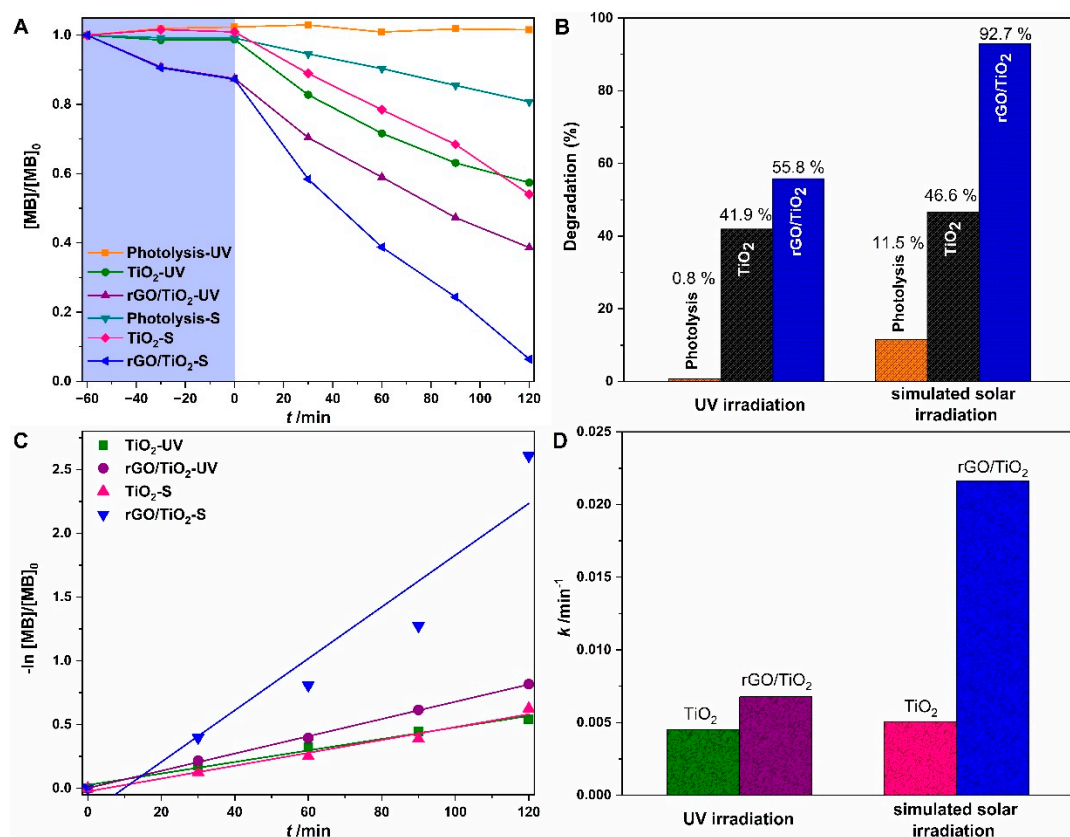


Figure 4. (A) Adsorption, photolytic and photocatalytic degradation of MB from an aqueous medium (milli-Q water) under ultraviolet-A (UV-A) and simulated solar irradiation (S) as a function of irradiation time. (B) photodegradation efficiency of photolytic and photocatalytic degradation of MB after 120 min. (C) the $-\ln [MB]/[MB]_0$ versus reaction time, and (D) kinetic rate constants of photocatalytic reactions by immobilised rGO/TiO_2 nanocomposite photocatalyst.

It can be seen that the adsorption of MB for immobilised pure TiO_2 photocatalyst was negligible, while slight adsorption capacity of MB on the surface of immobilised rGO/TiO_2 photocatalyst was observed (approximately 10%) after 60 min stirring in the dark. This phenomenon can be attributed to the strong π - π interactions between the benzene rings of MB structure and the aromatic surface of rGO nanosheets, which clearly contribute to the pollutants' adsorption [38].

After 120 min of UV-A irradiation, the photodegradation efficiency of bare TiO_2 and rGO/TiO_2 photocatalysts is about 41.9% and 55.8% for MB dye from an aqueous medium (milli-Q water), whereas the same photocatalyst shows increased photodegradation efficiency under simulated solar irradiation to about 46.6% and 92.7%, respectively. The obtained photodegradation results demonstrate that the immobilised rGO/TiO_2 nanocomposite has superior photocatalytic activity, particularly under simulated solar irradiation.

The photodegradation rate constant (k) can be calculated by extrapolating time-dependent degradation function in a logarithmic relation i.e., of $-\ln (c/c_0)$ versus irradiation time (t) as shown in Figure 4C. The obtained results for UV-A irradiation were as follows: 0.00452 min^{-1} and 0.00677 min^{-1} for pure TiO_2 and rGO/TiO_2 nanocomposite, respectively. The obtained linear correlation coefficient (R^2) was 0.9874 and 0.9991 for pure TiO_2 and rGO/TiO_2 nanocomposite, respectively. The obtained results for simulated solar

irradiation were as follows: 0.005 min^{-1} and 0.0171 min^{-1} for pure TiO_2 and rGO/TiO_2 nanocomposite, respectively (Figure 4D). The obtained linear correlation coefficient (R^2) was 0.9788 and 0.9859 for pure TiO_2 and rGO/TiO_2 nanocomposite, respectively. The photodegradation rate constant of all tested materials follows the first-order kinetic rate. The obtained values of the first-order rate constant and the photocatalytic degradation efficiency decrease in the following order: $\text{rGO}/\text{TiO}_2 > \text{TiO}_2$ for both irradiation sources (ultraviolet and simulated solar light). The enhanced photocatalytic degradation of MB dye from an aqueous medium (milli-Q water) at natural pH may be due to the high light intensity of simulated solar irradiation where the intensity of the UV was $4.90 \pm 0.1 \text{ mW cm}^{-2}$ at a distance of 15 cm from the light source. On the other hand, the intensity of the UV-A lamp was significantly lower, $0.98 \pm 0.05 \text{ mW cm}^{-2}$ for the same experimental setup.

Several authors have reported the photocatalytic capabilities of rGO/TiO_2 nanocomposite in the form of suspension for the degradation of persistent organic pollutants such as dyes under different types of irradiation sources. Furthermore, they reported the high photocatalytic effectiveness of the rGO/TiO_2 nanocomposite in several studied systems [1,14,20,33,39,40].

Zouzelka et al. [10] studied the photocatalytic degradation of 4-chlorophenol while using immobilised TiO_2/rGO nanocomposite under UV irradiation. The authors reported degradation around 80% for 4-chlorophenol after 300 min irradiation, respectively. In another study, Viet et al. [41] investigated the capability of immobilised rGO/TiO_2 for degradation of MB under UV light irradiation. It was found that according to optimised experimental parameters, the photodegradation of MB was complete after 120 min.

Thus considered, our results for the immobilised rGO/TiO_2 nanocomposite are in good agreement with the reported studies. Moreover, immobilised rGO/TiO_2 nanocomposite in this study shows a high potential for photocatalytic application due to the possible use of natural sunlight irradiation. Furthermore, the use of immobilised rGO/TiO_2 photocatalyst is more cost-effective than in the form of suspension due to the high cost of separation.

Advanced oxidation processes are effective for the removal of organic pollutants, but the oxidation rates of the compounds may be mainly affected by the composition of the water matrix. The water matrix can play a crucial role in the rate of photodegradation reactions. Dissolved inorganic and organic species can act as promoters and/or inhibitors in the photocatalytic processes [42–44]. Adsorption and photocatalytic efficiency of MB dye in several water environments were investigated. The obtained results for MB dye degradation using immobilised rGO/TiO_2 nanocomposite, under solar-like irradiation, in milli-Q water, river water, lake water, and seawater, are shown in Figure 5. It can be observed that the adsorption efficiency of MB on the surface of immobilised rGO/TiO_2 nanocomposite was higher in all monitored water matrices (river, sea, and lake) than in milli-Q water. The obtained adsorption of MB was ~10%, 20%, 21%, and 24% for milli-Q water, lake water, river water, and sea water, respectively (Figure 5A). In all the samples, almost complete photodegradation of MB dye was observed after 120 min. At the end of the photocatalytic reaction, 92.7%, 96.1%, 93.3%, and 84.9% of MB dye concentrations were removed from milli-Q water, river water, lake water, and sea water, respectively, as shown in Figure 5B. As noted, a significant increase of MB dye degradation was observed in the sample of river water using immobilised rGO/TiO_2 nanocomposite under simulated solar irradiation. The enhanced degradation of MB in the river water matrix may be due to a small amount of ions that can affect the photodegradation of MB dye [43,45]. It was found that degradation of MB dye in lake and milli-Q water samples is very similar. The lowest photodegradation of MB was obtained in the seawater sample. Seawater usually contains a large amount of inorganic salts (especially NaCl) which can have a negative impact on the photocatalyst activity. The deactivation of the photocatalyst by inorganic species in the seawater matrix has been connected with free radicals and the active sites on the catalyst surface are thus terminated [42,46]. The reaction rate constant (k) was calculated again from the slope of a plot between $\ln(C/C_0)$ and reaction time (t) as shown in Figure 5C,D. The obtained results for different water matrices were as follows: 0.0216 min^{-1} , 0.02732 min^{-1} , 0.02232 min^{-1} ,

and 0.01601 min^{-1} for milli-Q, river, lake, and seawater matrices, respectively (Figure 5D). It was observed that immobilised rGO/TiO₂ nanocomposite can play an important role in the efficient and fast photocatalytic degradation of MB dye in several aquatic matrices.

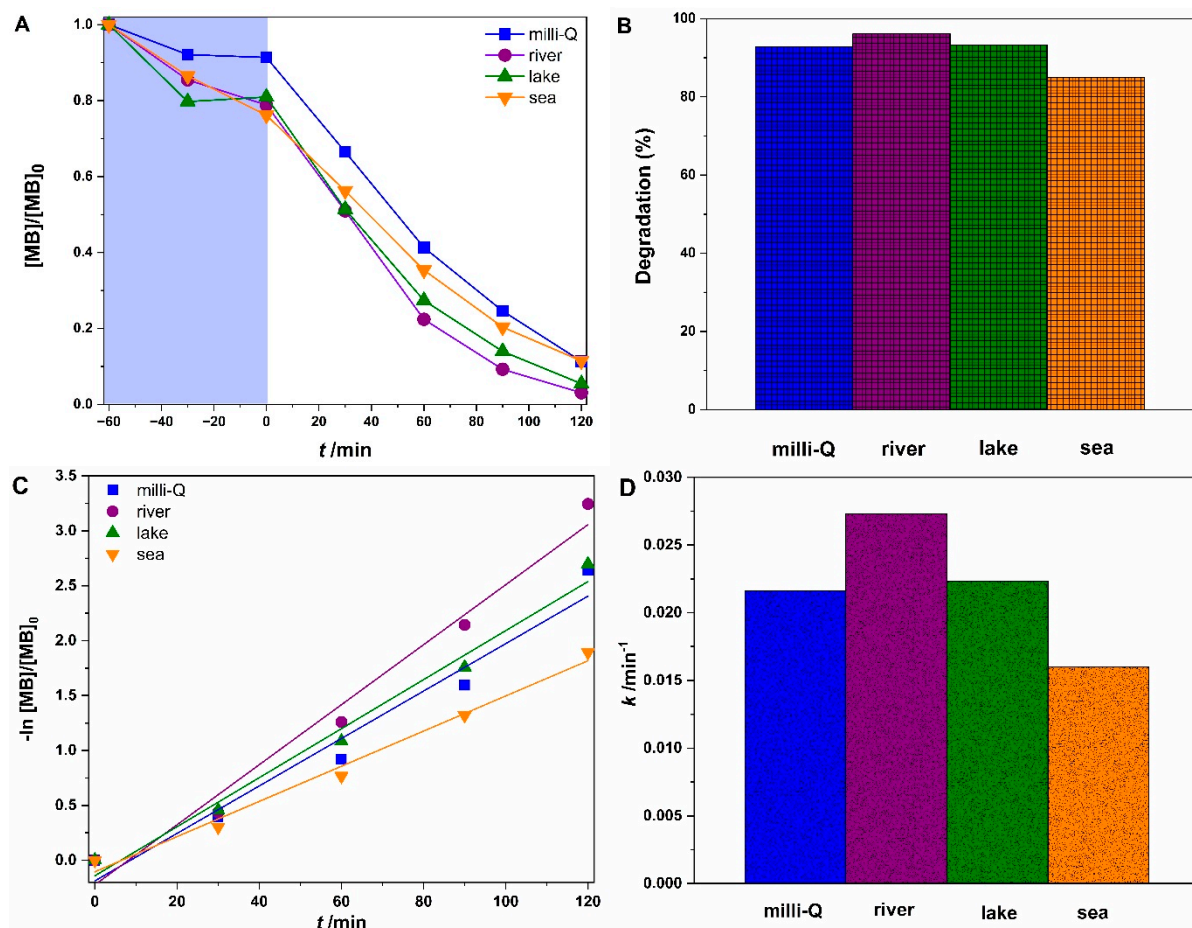


Figure 5. Effect of different water matrices (milli-Q water, river water, seawater, and lake water) on the (A) adsorption (stirring in the dark) and photodegradation efficiency of MB dye using rGO/TiO₂ nanocomposite under solar-like irradiation, (B) degradation efficiency of MB, (C) the $-\ln [MB]/[MB]_0$ versus reaction time, and (D) kinetic rate constants of photocatalytic reaction in different environmental water matrices.

The improved photocatalytic activity of the immobilised rGO/TiO₂ photocatalyst may be described by an increased establishment of radicals leading to a better separation of charge carriers. These conditions can be created by the presence of rGO material repressing the recombination of the charge carrier. The recombination may be achieved over the graphene surface due to the high mobility of electrons. Furthermore, freed oxidative holes can directly react with the organic pollutant compounds or indirectly through the OH radicals, which are strong oxidants [39,47]. Active components such as hydroxyl radical ($\bullet\text{OH}$), hole (h^+), and electron (e^-) play different roles in the photocatalytic degradation of organic dyes. For example, the reduction of e^- may demolish the double bond in the structure of organic dyes [33,48]. To investigate the role of different hydroxyl radical in the photocatalytic degradation of MB in an aqueous medium (milli-Q water), identical catalytic experiments have been carried out in the presence of isopropanol (IPA), AgNO₃, and EDTA-2Na, as shown in Figure 6. IPA rapidly reacts with hydroxyl radical and because these radicals are terminated, we can determine the role of hydroxyl radical in photocatalytic reactions [47]. In this case, it was observed that the photodegradation efficiency increases with the presence of isopropanol; to be precise, with 0.01 mol L^{-1} of isopropanol, the process efficiency

increases by 4.5% after reaction duration of 120 min compared to the MB degradation without the presence of active species. If hydroxyl radicals were the primary species leading to the degradation of MB during immobilised rGO/TiO₂ photocatalyst, the addition of isopropanol should inhibit the photodegradation. The minimal level of increase observed upon addition of hydroxyl radical indicates that the hydroxyl-radical-based oxidation pathway does not play a significant role in the degradation of MB with immobilised rGO/TiO₂ nanocomposite photocatalyst under simulated solar irradiation [49–52]. To determine the presence of h⁺ and e⁻ in photodegradation of MB, EDTA-2Na and AgNO₃ were used as an active species. The inhibition of MB degradation in the presence of EDTA-2Na is decreased by 11% compared with the photodegradation efficiency of MB without addition of active species. This suggests that holes are an important factor in our catalytic process. On the other hand, addition of AgNO₃ is less effective and even slightly increases the degradation by 0.7%. The photodegradation rates changed regarding the active component which is added in the photocatalytic process. The active species of photocatalytic activity for immobilised rGO/TiO₂ follows the order: h⁺ > none > e⁻ > •OH. It can be concluded that only addition of EDTA-2Na, a hole scavenger, inhibited the photocatalytic degradation of MB using immobilised rGO/TiO₂ nanocomposite. Based on obtained experimental results, the decreased photodegradation efficiency suggested that the photocatalytic activity of immobilised rGO/TiO₂ nanocomposite under simulated solar irradiation for removal of MB is driven by the presence of a hole, similarly as in [33,52–55].

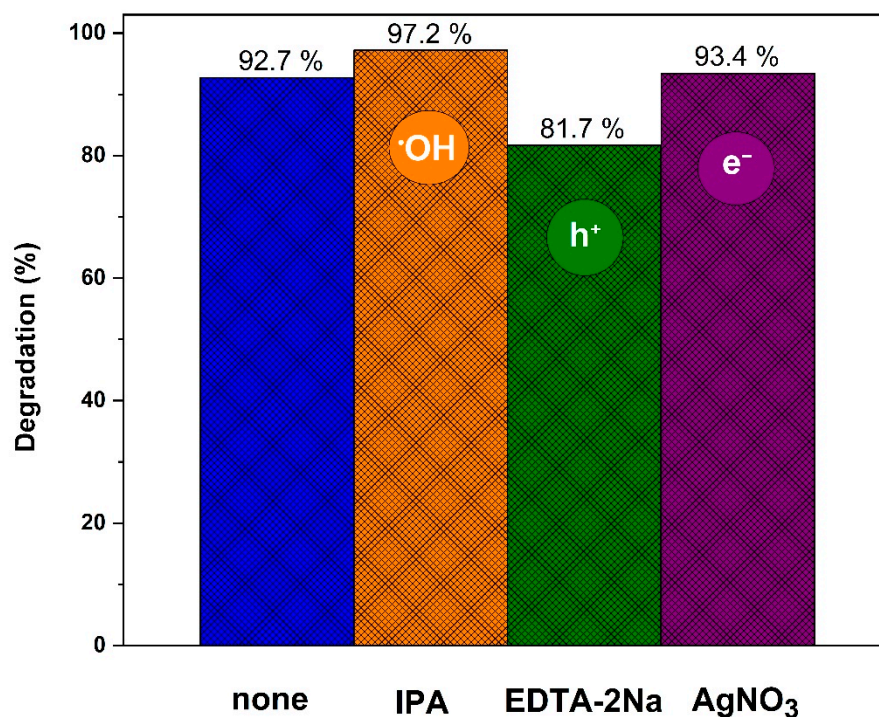


Figure 6. Effects of scavengers on the degradation of MB dye in milli-Q water with scavenger dosage of 0.01 mol L⁻¹ after 120 min of simulated solar irradiation.

For the reusability investigation of the immobilised photocatalyst, the photoactivity was carried out by five consecutive cycles of MB removal from an aqueous medium (milli-Q water) within 30 min intervals for 120 min of irradiation using simulated solar light. Figure 7 shows the results of the immobilised rGO/TiO₂ photocatalyst. After five cycles, the photodegradation of MB is slightly decreased, 92.7%, 92.9%, 92.5%, 92.6%, and 91.3%, respectively. The obtained results show very high reusability of immobilised rGO/TiO₂ photocatalyst for removal after each cycle. The reason for such robust appearance is probably due to the strong interaction between photocatalyst and adhesive material (ethylene glycol) where the photocatalyst remained attached to the substrate after five consecutive

cycles. The obtained results clearly indicate the high chemical and operating stability of the immobilised rGO/TiO₂ photocatalyst and point towards significant reusability as a photocatalyst. Moreover, these results are in striking contrast to our previous report where the rGO/TiO₂ powder photodegradation efficiency was decreased because the amount of catalyst was lost between the consecutive cycles [56].

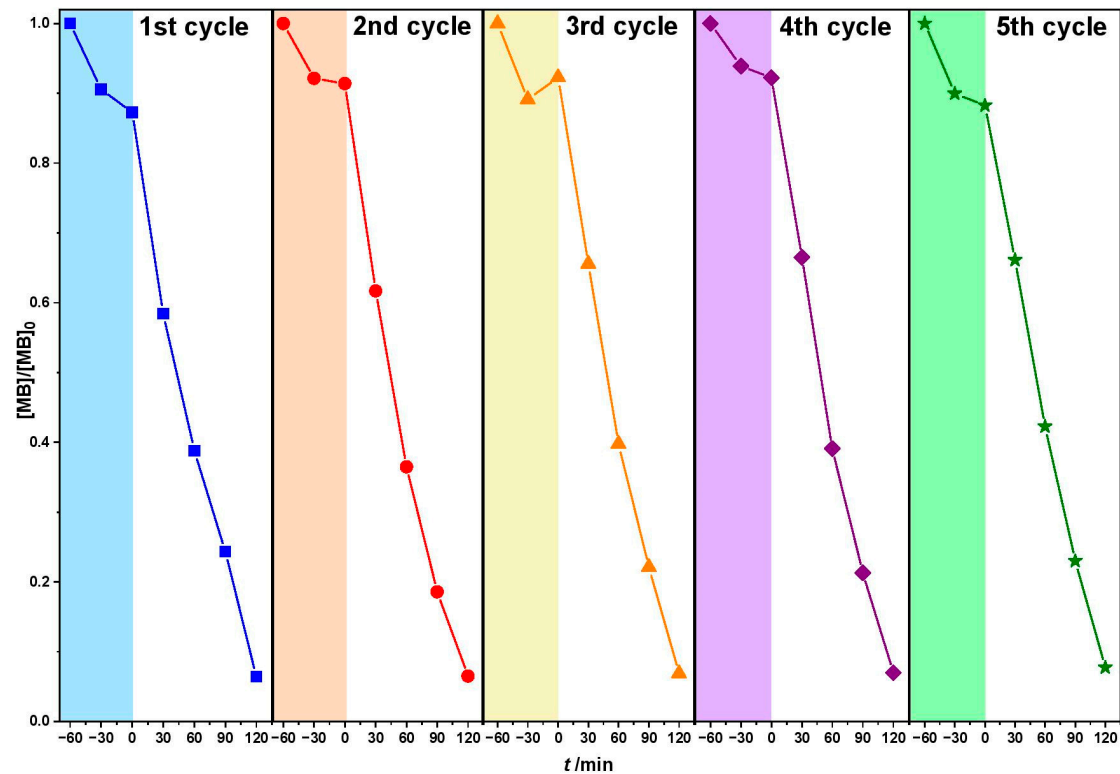


Figure 7. The recyclability of immobilised rGO/TiO₂ photocatalyst during removal of MB from an aqueous medium (milli-Q water) using simulated solar irradiation.

The proposed mechanism of photocatalytic degradation by rGO/TiO₂ nanocomposite is shown in Figure 8. rGO material in the rGO/TiO₂ nanocomposite can improve photocatalytic degradation of MB by promoting separation and charge transfer. The electron-hole pairs have been excited within the TiO₂ molecule after UV-Vis irradiation. The electrons (e⁻) can be quickly shifted from the conductive band (CB) of the TiO₂ molecule to the surface of the rGO material. Then, transferred electrons in combination with present oxygen will favour the radical O₂^{•-}. Produced O₂^{•-} has the potential to react with H₂O/H⁺ to form [•]OH radical, which is the primary radical in the degradation of MB dye. In the meantime, the holes (h⁺) on the valence band (VB) of the TiO₂ molecule have the potential to oxidise H₂O/OH⁻ to also form [•]OH radicals [33,57,58].

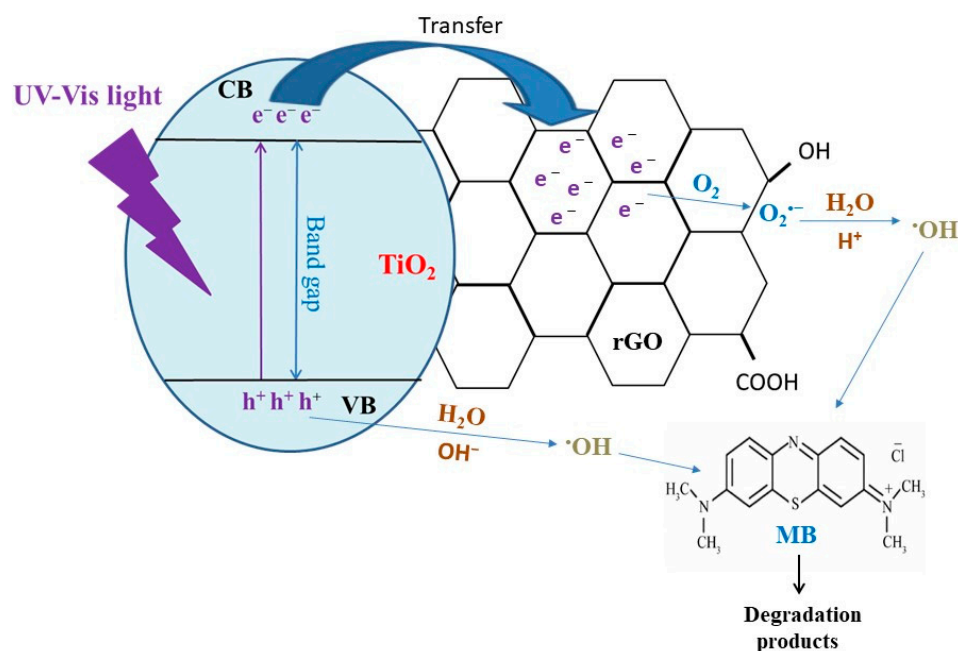


Figure 8. The photocatalytic mechanisms of rGO/TiO₂ nanocomposite for MB dye degradation.

4. Conclusions

In the framework of this work, a simple and efficient approach to preparing rGO/TiO₂ immobilised nanocomposite is presented. The photocatalytic activity of immobilised rGO/TiO₂ nanocomposite was verified by the photodegradation of methylene blue (MB) dye in aqueous solution under UV-A and simulated solar irradiations. It was found that the rate of MB photocatalytic degradation is higher by immobilised rGO/TiO₂ nanocomposite in comparison with immobilised pure TiO₂.

It was found that photocatalytic degradation of MB dye under solar-like irradiation in investigated water matrices follows the order: river > lake > milli-Q > seawater.

It was determined that holes (h⁺) play an important role in the photocatalytic activity of immobilised rGO/TiO₂ nanocomposite under simulated solar irradiation for the removal of MB dye.

The obtained photodegradation results show that the optimised immobilisation method shows promising result for the immobilisation of rGO/TiO₂ nanocomposite on a glass substrate with high photocatalytic performances for multi-cycle use (five cycles) up to 90%, which is of utmost significance for their implementation under real conditions.

Author Contributions: Conceptualisation, M.K., M.P., L.Č. and D.V.; methodology, M.K., L.Č. and M.P.; software, M.K., D.V. and M.P.; validation, M.K.; formal analysis, M.K. and M.P.; investigation, M.K.; resources, M.P.; data curation, M.K., L.Č. and M.P.; writing—original draft preparation, M.K., I.B., G.O.-I., M.J.H., T.R. and M.P.; writing—review and editing, L.Č., D.V., M.P. and G.G.; visualisation, M.K. and M.P.; supervision, L.Č. and M.P.; project administration, M.K., L.Č. and M.P.; funding acquisition, L.Č. and M.P. All authors have read and agreed to the published version of the manuscript.

Funding: This research received no external funding.

Institutional Review Board Statement: Not applicable.

Informed Consent Statement: Not applicable.

Data Availability Statement: Data sharing is not applicable to this article.

Acknowledgments: The present study was supported by the Slovenian Research Agency (ARRS) under the Contracts J2-9440, L2-1830, and P2-0084. G.G. gratefully acknowledges the Portuguese Science Foundation (FCT) for Programme Stimulus of Scientific Employment—Individual Support

(CEECIND/01913/2017) and financial support of TEMA by the projects UIDB/00481/2020 and UIDP/00481/2020; and CENTRO-01-0145-FEDER-022083—Centro Portugal Regional Operational Programme (Centro 2020), under the PORTUGAL 2020 Partnership Agreement, through the European Regional Development Fund. I.B. acknowledges support by the Portuguese Foundation for Science and Technology (FCT): IF/00582/2015.

Conflicts of Interest: The authors declare no conflict of interest.

References

- Al-Mamun, M.R.; Kader, S.; Islam, M.S.; Khan, M.Z.H. Photocatalytic activity improvement and application of UV-TiO₂ photocatalysis in textile wastewater treatment: A review. *J. Environ. Chem. Eng.* **2019**, *7*. [CrossRef]
- Kant, R. Textile dyeing industry an environmental hazard. *Nat. Sci.* **2012**, *4*, 22–26. [CrossRef]
- Weber, E.J.; Adams, R.L. Chemical- and Sediment-Mediated Reduction of the Azo Dye Disperse Blue 79. *Environ. Sci. Technol.* **1995**, *29*, 1163–1170. [CrossRef]
- Turner, R.D.R.; Warne, M.S.J.; Dawes, L.A.; Thompson, K.; Will, G.D. Greywater irrigation as a source of organic micro-pollutants to shallow groundwater and nearby surface water. *Sci. Total Environ.* **2019**, *669*, 570–578. [CrossRef]
- Vembuli, T.; Thiripuranthagan, S.; Sureshkumar, T.; Erusappan, E.; Kumaravel, S.; Kasinathan, M.; Natesan, B.; Sivakumar, A. Degradation of Harmful Organics Using Visible Light Driven N-TiO₂/rGO Nanocomposite. *J. Nanosci. Nanotechnol.* **2021**, *21*, 3081–3091. [CrossRef] [PubMed]
- Tu, W.; Zhou, Y.; Zou, Z. Versatile graphene-promoting photocatalytic performance of semiconductors: Basic principles, synthesis, solar energy conversion, and environmental applications. *Adv. Funct. Mater.* **2013**, *23*, 4996–5008. [CrossRef]
- Chabot, V.; Higgins, D.; Yu, A.; Xiao, X.; Chen, Z.; Zhang, J. A review of graphene and graphene oxide sponge: Material synthesis and applications to energy and the environment. *Energy Environ. Sci.* **2014**, *7*, 1564–1596. [CrossRef]
- Avouris, P. Graphene: Electronic and photonic properties and devices. *Nano Lett.* **2010**, *10*, 4285–4294. [CrossRef] [PubMed]
- Li, F.; Jiang, X.; Zhao, J.; Zhang, S. Graphene oxide: A promising nanomaterial for energy and environmental applications. *Nano Energy* **2015**, *16*, 488–515. [CrossRef]
- Zouzelka, R.; Remzova, M.; Plsek, J.; Brabec, L.; Rathousky, J. Immobilized rGO/TiO₂ photocatalyst for decontamination of water. *Catalysts* **2019**, *9*, 708. [CrossRef]
- Gao, W. *Synthesis, Structure, and Characterizations*; Springer International Publishing: Cham, Switzerland, 2015; ISBN 9783319155005.
- Pei, S.; Cheng, H.M. The reduction of graphene oxide. *Carbon N. Y.* **2012**, *50*, 3210–3228. [CrossRef]
- Leal, J.F.; Cruz, S.M.A.; Almeida, B.T.A.; Esteves, V.I.; Marques, P.A.A.P.; Santos, E.B.H. TiO₂-rGO nanocomposite as an efficient catalyst to photodegrade formalin in aquaculture's waters, under solar light. *Environ. Sci. Water Res. Technol.* **2020**, *6*, 1018–1027. [CrossRef]
- Liu, Y. Hydrothermal synthesis of TiO₂-RGO composites and their improved photocatalytic activity in visible light. *RSC Adv.* **2014**, *4*, 36040–36045. [CrossRef]
- Harikrishnan, M.M.; Athira, S.; Sykam, N.; Mohan Rao, G.; Mathew, A. Preparation of rGO-TiO₂ Composite and Study of its Dye Adsorption Properties. *Mater. Today Proc.* **2019**, *9*, 61–69. [CrossRef]
- Kocijan, M.; Ćurković, L.; Ljubas, D.; Mužina, K.; Bačić, I.; Radošević, T.; Podlogar, M.; Bdkin, I.; Otero-Irurueta, G.; Hortigüela, M.J.; et al. Graphene-Based TiO₂ Nanocomposite for Photocatalytic Degradation of Dyes in Aqueous Solution under Solar-Like Radiation. *Appl. Sci.* **2021**, *11*, 3966. [CrossRef]
- An, X.; Yu, J.C. Graphene-based photocatalytic composites. *RSC Adv.* **2011**, *1*, 1426–1434. [CrossRef]
- Xiang, Q.; Yu, J.; Jaroniec, M. Graphene-based semiconductor photocatalysts. *Chem. Soc. Rev.* **2012**, *41*, 782–796. [CrossRef] [PubMed]
- Dąbrowski, A. Adsorption—From theory to practice. *Adv. Colloid Interface Sci.* **2001**, *93*, 135–224. [CrossRef]
- Sriwong, C.; Choojun, K.; Tejangkura, W.; Prasanseang, W. Preparation and photocatalytic activities of TiO₂-rGO nanocomposite catalysts for mb dye degradation over sunlight irradiation. *Mater. Sci. Forum* **2018**, *936*, 47–52. [CrossRef]
- Cheshme Khavar, A.H.; Moussavi, G.; Mahjoub, A.R. The preparation of TiO₂@rGO nanocomposite efficiently activated with UVA/LED and H₂O₂ for high rate oxidation of acetaminophen: Catalyst characterization and acetaminophen degradation and mineralization. *Appl. Surf. Sci.* **2018**, *440*, 963–973. [CrossRef]
- Cunha, D.L.; Kuznetsov, A.; Achete, C.A.; Machado, A.E.d.H.; Marques, M. Immobilized TiO₂ on glass spheres applied to heterogeneous photocatalysis: Photoactivity, leaching and regeneration process. *PeerJ* **2018**, *2018*, 1–19. [CrossRef]
- Lei, P.; Wang, F.; Gao, X.; Ding, Y.; Zhang, S.; Zhao, J.; Liu, S.; Yang, M. Immobilization of TiO₂ nanoparticles in polymeric substrates by chemical bonding for multi-cycle photodegradation of organic pollutants. *J. Hazard. Mater.* **2012**, *227–228*, 185–194. [CrossRef]
- Chong, M.N.; Tneu, Z.Y.; Poh, P.E.; Jin, B.; Aryal, R. Synthesis, characterisation and application of TiO₂-zeolite nanocomposites for the advanced treatment of industrial dye wastewater. *J. Taiwan Inst. Chem. Eng.* **2015**, *50*, 288–296. [CrossRef]
- Corredor, J.; Perez-Peña, E.; Rivero, M.J.; Ortiz, I. Performance of rGO/TiO₂ photocatalytic membranes for hydrogen production. *Membranes* **2020**, *10*, 218. [CrossRef]

26. Yildiz, T.; Yatmaz, H.C.; Öztürk, K. Anatase TiO₂ powder immobilized on reticulated Al₂O₃ ceramics as a photocatalyst for degradation of RO16 azo dye. *Ceram. Int.* **2020**, *46*, 8651–8657. [\[CrossRef\]](#)
27. Abd-Elrahim, A.G.; Chun, D.M. Room-temperature deposition of ZnO-graphene nanocomposite hybrid photocatalysts for improved visible-light-driven degradation of methylene blue. *Ceram. Int.* **2021**, *47*, 12812–12825. [\[CrossRef\]](#)
28. Švagelj, Z.; Mandić, V.; Čurković, L.; Biošić, M.; Žmak, I.; Gaborardi, M. Titania-Coated Alumina Foam Photocatalyst for Memantine Degradation Derived by Replica Method and Sol-Gel Reaction. *Materials* **2020**, *13*, 227. [\[CrossRef\]](#) [\[PubMed\]](#)
29. Fan, H.; Yi, G.; Zhang, X.; Xing, B.; Zhang, C.; Chen, L.; Zhang, Y. Facile synthesis of uniformly loaded Fe₃O₄-TiO₂/rGO ternary hybrids for enhanced photocatalytic activities. *Opt. Mater.* **2021**, *111*, 110582. [\[CrossRef\]](#)
30. Mokhtarifar, M.; Kaveh, R.; Bagherzadeh, M.; Lucotti, A.; Pedferri, M.P.; Diamanti, M.V. Heterostructured TiO₂/SiO₂/γ-Fe₂O₃/rGO Coating with Highly Efficient Visible-Light-Induced Self-Cleaning Properties for Metallic Artifacts. *ACS Appl. Mater. Interfaces* **2020**, *12*, 29671–29683. [\[CrossRef\]](#) [\[PubMed\]](#)
31. Gabelica, I.; Čurković, L.; Mandić, V.; Panžić, I.; Ljubas, D.; Zadro, K. Rapid Microwave-Assisted Synthesis of Fe₃O₄/SiO₂/TiO₂ Core-2-Layer-Shell Nanocomposite for Photocatalytic Degradation of Ciprofloxacin. *Catalysts* **2021**, *11*, 1136. [\[CrossRef\]](#)
32. Čurković, L.; Ljubas, D.; Šegota, S.; Bačić, I. Photocatalytic degradation of Lissamine Green B dye by using nanostructured sol-gel TiO₂ films. *J. Alloys Compd.* **2014**, *604*, 309–316. [\[CrossRef\]](#)
33. Li, T.; Wang, T.; Qu, G.; Liang, D.; Hu, S. Synthesis and photocatalytic performance of reduced graphene oxide-TiO₂ nanocomposites for orange II degradation under UV light irradiation. *Environ. Sci. Pollut. Res.* **2017**, *24*, 12416–12425. [\[CrossRef\]](#)
34. Arumugam, P.; Sengodan, P.; Duraisamy, N.; Rajendran, R.; Vasudevan, V. An effective strategy to enhance the photocatalytic performance by forming NiS/rGO heterojunction nanocomposites. *Ionics* **2020**, *26*, 4201–4212. [\[CrossRef\]](#)
35. Ruidíaz-Martínez, M.; Álvarez, M.A.; López-Ramón, M.V.; Cruz-Quesada, G.; Rivera-Utrilla, J.; Sánchez-Polo, M. Hydrothermal Synthesis of rGO-TiO₂ Composites as High-Performance UV Photocatalysts for Ethylparaben Degradation. *Catalysts* **2020**, *10*, 520. [\[CrossRef\]](#)
36. Pastrana-Martínez, L.M.; Morales-Torres, S.; Likodimos, V.; Figueiredo, J.L.; Faria, J.L.; Falaras, P.; Silva, A.M.T. Advanced nanostructured photocatalysts based on reduced graphene oxide-TiO₂ composites for degradation of diphenhydramine pharmaceutical and methyl orange dye. *Appl. Catal. B Environ.* **2012**, *123–124*, 241–256. [\[CrossRef\]](#)
37. Čizmić, M.; Ljubas, D.; Čurković, L.; Škorić, I.; Babić, S. Kinetics and degradation pathways of photolytic and photocatalytic oxidation of the anthelmintic drug praziquantel. *J. Hazard. Mater.* **2017**, *323*, 500–512. [\[CrossRef\]](#)
38. Qin, Y.L.; Zhao, W.W.; Sun, Z.; Liu, X.Y.; Shi, G.L.; Liu, Z.Y.; Ni, D.R.; Ma, Z.Y. Photocatalytic and adsorption property of ZnS-TiO₂/rGO ternary composites for methylene blue degradation. *Adsorpt. Sci. Technol.* **2019**, *37*, 764–776. [\[CrossRef\]](#)
39. Garrafa-Gálvez, H.E.; Alvarado-Beltrán, C.G.; Almaral-Sánchez, J.L.; Hurtado-Macias, A.; Garzon-Fontecha, A.M.; Luque, P.A.; Castro-Beltrán, A. Graphene role in improved solar photocatalytic performance of TiO₂-rGO nanocomposite. *Chem. Phys.* **2019**, *521*, 35–43. [\[CrossRef\]](#)
40. Kumar, V.; Bansal, A.; Gupta, R. *Synthesis of rGO/TiO₂ Nanocomposite for the Efficient Photocatalytic Degradation of RhB Dye*; Springer: Singapore, 2019; Volume 30, ISBN 9789811367175.
41. Viet, T.Q.Q.; Nhu, T.H.; Thinh, D.B.; Trinh, D.N.; Giang, N.T.H.; Dat, N.M.; Hai, N.D.; Nam, H.M.; Phong, M.T.; Hieu, N.H. Optimization of TiO₂ immobilized—Reduce graphene oxide photocatalyst toward organic compounds in aqueous medium. *Synth. Met.* **2021**, *280*, 116867. [\[CrossRef\]](#)
42. Lado Ribeiro, A.R.; Moreira, N.F.F.; Li Puma, G.; Silva, A.M.T. Impact of water matrix on the removal of micropollutants by advanced oxidation technologies. *Chem. Eng. J.* **2019**, *363*, 155–173. [\[CrossRef\]](#)
43. Yang, Y.; Zhang, Y.; Gou, C.; Wu, W.; Wang, H.; Zeng, Q. Solar photocatalytic degradation of thidiazuron in Yangtze River water matrix by Ag/AgCl-AC at circumneutral condition. *Environ. Sci. Pollut. Res.* **2020**, *27*, 40857–40869. [\[CrossRef\]](#) [\[PubMed\]](#)
44. Jiménez-Salcedo, M.; Monge, M.; Tena, M.T. The photocatalytic degradation of sodium diclofenac in different water matrices using g-C₃N₄ nanosheets: A study of the intermediate by-products and mechanism. *J. Environ. Chem. Eng.* **2021**, *9*, 105827. [\[CrossRef\]](#)
45. Zafar, Z.; Fatima, R.; Kim, J.O. Experimental studies on water matrix and influence of textile effluents on photocatalytic degradation of organic wastewater using Fe-TiO₂ nanotubes: Towards commercial application. *Environ. Res.* **2021**, *197*, 111120. [\[CrossRef\]](#) [\[PubMed\]](#)
46. Rioja, N.; Zorita, S.; Peñas, F.J. Effect of water matrix on photocatalytic degradation and general kinetic modeling. *Appl. Catal. B Environ.* **2016**, *180*, 330–335. [\[CrossRef\]](#)
47. Pelaez, M.; Falaras, P.; Likodimos, V.; O'Shea, K.; de la Cruz, A.A.; Dunlop, P.S.M.; Byrne, J.A.; Dionysiou, D.D. Use of selected scavengers for the determination of NF-TiO₂ reactive oxygen species during the degradation of microcystin-LR under visible light irradiation. *J. Mol. Catal. A Chem.* **2016**, *425*, 183–189. [\[CrossRef\]](#) [\[PubMed\]](#)
48. Zhang, W.; Xiao, X.; Zeng, X.; Li, Y.; Zheng, L.; Wan, C. Enhanced photocatalytic activity of TiO₂ nanoparticles using SnS₂/RGO hybrid as co-catalyst: DFT study and photocatalytic mechanism. *J. Alloys Compd.* **2016**, *685*, 774–783. [\[CrossRef\]](#)
49. Maruthamani, D.; Divakar, D.; Kumaravel, M. Enhanced photocatalytic activity of TiO₂ by reduced graphene oxide in mineralization of Rhodamine B dye. *J. Ind. Eng. Chem.* **2015**, *30*, 33–43. [\[CrossRef\]](#)
50. Duan, Y.; Gou, M.L.; Guo, Y.; Cai, J.; Song, W.; Liu, Z.; Zhou, E. In situ hydrothermal synthesis of TiO₂-rGO nanocomposites for 4-nitrophenol degradation under sunlight irradiation. *J. Mater. Res.* **2021**, *36*, 906–915. [\[CrossRef\]](#)

51. Zhang, Q.; Zhang, Y.; Meng, Z.; Tong, W.; Yu, X.; An, Q. Constructing the magnetic bifunctional graphene/titania nanosheet-based composite photocatalysts for enhanced visible-light photodegradation of MB and electrochemical ORR from polluted water. *Sci. Rep.* **2017**, *7*, 1–12. [[CrossRef](#)]
52. Tju, H.; Taufik, A.; Saleh, R. Enhanced UV Photocatalytic Performance of Magnetic Fe₃O₄/CuO/ZnO/NGP Nanocomposites. *J. Phys. Conf. Ser.* **2016**, *710*. [[CrossRef](#)]
53. Li, Y.; Xiao, X.; Ye, Z. Facile fabrication of tetragonal scheelite (t-s) BiVO₄/g-C₃N₄ composites with enhanced photocatalytic performance. *Ceram. Int.* **2018**, *44*, 7067–7076. [[CrossRef](#)]
54. Liu, Y.; Shi, Y.; Zhang, S.; Liu, B.; Sun, X.; Yang, D. Optimizing the interface of C/titania@reduced graphene oxide nanofibers for improved photocatalytic activity. *J. Mater. Sci.* **2019**, *54*, 8907–8918. [[CrossRef](#)]
55. Van Hung, N.; Nguyet, B.T.M.; Nghi, N.H.; Khieu, D.Q. Photocatalytic Degradation of Methylene Blue by Using ZnO/Longan Seed Activated Carbon Under Visible-Light Region. *J. Inorg. Organomet. Polym. Mater.* **2021**, *31*, 446–459. [[CrossRef](#)]
56. Kocijan, M.; Ćurković, L.; Radošević, T.; Podlogar, M. Enhanced Photocatalytic Activity of Hybrid rGO@TiO₂/CN Nanocomposite for Organic Pollutant Degradation under Solar Light Irradiation. *Catalysts* **2021**, *11*, 1023. [[CrossRef](#)]
57. Wang, P.; Wang, J.; Wang, X.; Yu, H.; Yu, J.; Lei, M.; Wang, Y. One-step synthesis of easy-recycling TiO₂-rGO nanocomposite photocatalysts with enhanced photocatalytic activity. *Appl. Catal. B Environ.* **2013**, *132–133*, 452–459. [[CrossRef](#)]
58. Lei, M.; Wang, N.; Zhu, L.; Xie, C.; Tang, H. A peculiar mechanism for the photocatalytic reduction of decabromodiphenyl ether over reduced graphene oxide-TiO₂ photocatalyst. *Chem. Eng. J.* **2014**, *241*, 207–215. [[CrossRef](#)]